Journal of Hydroinformatics

Journal of Hydroinformatics Vol 26 No 7, 1790 doi: 10.2166/hydro.2024.137

Experiments on flow velocity profiles in mountain river channels

Jia Peng[a,b], Dong Chen[a,b,*], Shizhengxiong Liang[a,b], Rongcai Tang[c], Hong Hu[c] and Hang Wang[c]

[a] Key Laboratory of Water Cycle and Related Land Surface Processes, Institute of Geographic Sciences and Natural Resources Research, Chinese Academy of Sciences, Beijing, China
[b] College of Resources and Environment, University of Chinese Academy of Sciences, Beijing, China
[c] State Key Laboratory of Hydraulics and Mountain River Engineering, Sichuan University, Chengdu, China
*Corresponding author. E-mail: dchen@igsnrr.ac.cn

JP, 0009-0009-3922-7652

ABSTRACT

Research on the vertical profiles of flow velocity in mountainous river channels is limited, particularly in scenarios where complex bed geometries are absent. Due to the coarse roughness and seepage flow on streambeds composed of gravel, the conventional formulae for flow velocity profiles derived from fluvial river channels do not apply to mountainous river channels. Based on flume experiments with a bed packed with natural gravel and a slope ranging from 0.006 to 0.16, we derived a theoretical formula for flow velocity profiles. This new formula integrates the influence of the subsurface flow and velocity reduction near the water surface, demonstrating a strong alignment with measurements. Our findings indicate that for shallow water flow over rough bed surfaces, the turbulence intensity diminishes along the vertical direction in the near-bed region while remaining relatively constant in the upper water body. Contrary to conventional theories which attribute the increase in flow resistance and the decrease in sediment transport rates in mountainous river channels to form drag, our study emphasizes that the subsurface flow plays a significant role in the overall flow resistance of mountainous river channels and should not be overlooked.

Key words: flow resistance, mountainous river channels, subsurface flow, velocity vertical profiles

HIGHLIGHTS

- The comprehension of flow velocity profiles in mountainous river channels remains limited, especially in scenarios with subsurface flow and secondary flow.
- Study challenges conventional theories by highlighting the significant role of subsurface flow in overall flow resistance and sediment transport rates in mountainous river channels.

GRAPHICAL ABSTRACT

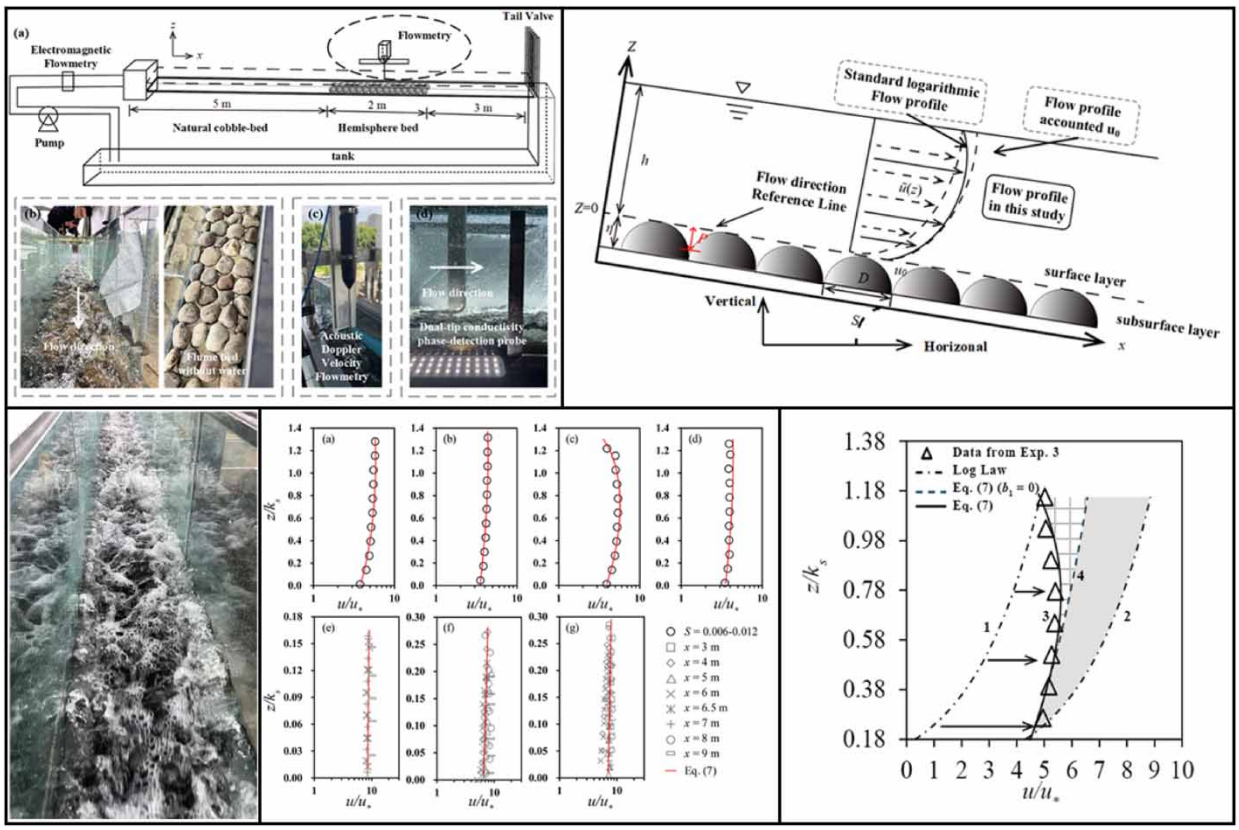

NOTATIONS

D_{50}	median particle size
D_{84}	particle size of which 84% are finer
k_s	roughness height
S	flume bed slope
Q	discharge
W	flume width
Re	Reynolds number
Re_{ks}	roughness Reynolds number
Fr	Froude number
U	average velocity
u_0	seepage velocity at the bed surface
u_*	bed shear velocity
$\bar{u}$	downstream velocity averaged in time
L_t	mixing length
ε	Eddy viscosity
g	gravity acceleration
h	water depth
P	thickness of exchange layer
η	thickness of subsurface layer
R	specific density
x, y, z	flume reference frame
τ	shear stress
τ_*	bed shear stress
α_1, b_1	coefficients of Equation (7)

INTRODUCTION

In open-channel flows, the vertical profiles of flow velocity have been extensively studied by numerous researchers (Finley *et al.* 1966; Nezu & Rodi 1986; Wiberg & Smith 1991; Ferro & Baiamonte 1994; Ferro 2003; Wang *et al.* 2015; Lamb *et al.* 2017a, 2017b; Luo *et al.* 2020, 2022), resulting in various forms of velocity profile formulae, including logarithmic (Nezu & Rodi 1986; Wiberg & Smith 1991; Lamb *et al.* 2017b; Luo *et al.* 2022), hyperbolic tangent (Luo *et al.* 2020), and irregular forms (Finley *et al.* 1966; Ferro & Baiamonte 1994; Ferro 2003; Wang *et al.* 2015). Among these, the logarithmic formulae are the most widely applied. However, to date, most studies on velocity profiles have focused on alluvial channels with gentle slopes. Due to the difficulty in integrating the influence of bed roughness and subsurface flow (Yager *et al.* 2012; Heimann *et al.* 2015; Schneider *et al.* 2015), research on velocity profiles in mountainous river channels with steep slopes and rough bed surfaces remains limited. The present situation results in considerable uncertainty in its application, e.g., sediment transport (Ferguson 2007; Rickenmann & Recking 2011; Wu *et al.* 2023) microorganism transport (Li *et al.* 2023b) and contaminant transport (Jiang *et al.* 2022). When applying the conventional formulae of flow velocity profiles derived from fluvial river channels to estimate the sediment transport rates in mountainous river channels, the calculated results may differ by one to two orders of magnitude from actual measurements (Bathurst 2002; Barry *et al.* 2004; Yager *et al.* 2012). Owing to the complex geometric structures and shallow depths, velocity profiles in mountainous river channels exhibit non-conventional patterns (Wiberg & Smith 1991; Ferro & Baiamonte 1994; Ferro 2003; Wang *et al.* 2015). The streambeds of mountainous river channels are often characterized by gravels, pebbles, even boulders, and sometimes sediment aggregates and bedform morphology (Yager *et al.* 2007; Schneider *et al.* 2015), which may bring considerable subsurface flow and water surface waves (Finley *et al.* 1966; Ferro & Baiamonte 1994; Wang *et al.* 2015), subsequently influences velocity profiles.

In steep channels with gravel beds with relatively shallow flow depths, flow velocities near the bed remain relatively high due to significant subsurface flow, causing deviations from the standard logarithmic velocity profiles (Lamb *et al.* 2017b; Luo *et al.* 2020, 2022). Although sometimes velocity profiles on gravel-bed river channels can still be approximated by logarithmic formulas, there is no satisfactory method for determining parameters for different bed surfaces and slopes (Gupta & Paudyal 1985; Nakagawa *et al.* 1988; Tu *et al.* 1988). Some scholars have suggested to divide the vertical velocity structure into different regions, but this method is challenging due to the difficulty in determining the thickness of the bottom rough layer (Zagni & Smith 1976; Vedula & Achanta 1985). Lamb *et al.* (2017a, 2017b) considered variations in bed permeability and roughness across the entire flow depth and developed a one-dimensional velocity model coupling surface and subsurface flows for steep streams with planar rough beds. Luo *et al.* (2022) considered porosity parameters in his model and achieved numerical solutions for subsurface flow equations.

Field surveys in mountainous river channels indicate that 90% of velocity profile structures deviate from the logarithmic distribution (Byrd *et al.* 2000), including 'S'-shaped and Dean-Finley profiles (Ferro & Baiamonte 1994; Ferro & Pecoraro 2000). Through scale analysis of momentum and kinetic energy equations, Byrd *et al.* (2000) found that the 'S'-shaped profiles are mainly due to form drag associated with coarse bed roughness. Similar non-conventional velocity profiles can be observed in stream channels with submerged vegetation and large bedform morphologies (Nepf & Ghisalberti 2008; Hu *et al.* 2013; Wang *et al.* 2023; Behera *et al.* 2024). The above studies indicate that the logarithmic velocity distribution is related to small-scale roughness ($k_s/h < 0.1$, in which k_s is the roughness height) while non-conventional velocity profiles in mountainous channels are related to large-scale roughness ($k_s/h > 0.2$) (Lamb *et al.* 2017b). Gravel-bed surfaces, similar to turbulent structures in rigid vegetation (Nepf & Ghisalberti 2008), affect the entire water body, and may result in the shrink of boundary layers (Roy *et al.* 2004; Lu *et al.* 2021). Nikora *et al.* (2007) used Reynolds-averaged Navier–Stokes (RANS) equations to obtain morphological stresses similar to Reynolds stresses, finding that these morphological stresses and turbulence kinetic energy may be responsible for non-conventional velocity profiles. Bathurst (1988) proposed conditions for forming 'S'-shaped velocity profiles: a slope steepness (S) of approximately 0.01, a ratio of water depth (h) to bed surface particle size (D_{84}, representing particles larger than 84% of the bed) between 1.0 and 4.0, ensuring non-uniform distribution of bed particles. Ferro & Baiamonte (1994) and Ferro (2003) proposed a four-parameter equation (a combination of logarithmic and polynomial equations) to fit 'S'-shaped profiles. The calculation results of existing formulae for flow resistance in mountainous river channels often very widely (Bathurst 2002). This is partially due to variations in location and significant changes in geometric morphology. Lamb *et al.* (2017b) conducted experiments in steep-slope, flat-bed channels and derived a vertical velocity profile formula coupled with surface and subsurface flow. The derived relationship of resistance coefficients closely matched field observations, indicating the significant influence of subsurface flow (Emmett 1970; Lamb *et al.* 2017b; Luo *et al.* 2022) on

flow resistance in mountainous river channels. Similarly, it has been found that surface wave fluctuations also affect the vertical velocity structure in steep-slope shallow water (Emmett 1970; Abrahams & Parsons 1994). Nevertheless, there is limited research examining the impact of this flow on resistance coefficients. Furthermore, it is challenging to accurately measure the relationship between water flow and sediment transport on hillslopes (Qu *et al.* 2023).

The acoustic Doppler velocity flowmetry (ADV) has been widely used for velocity structure measurements. However, ADV is no longer suitable for velocity measurements for steep bed slopes and rough surfaces (Lamb *et al.* 2017b). Due to the presence of bubbles, measuring velocities in highly aerated flows is challenging, and the presence of a large amount of air in the water alters energy dissipation and flow transport. This study adopted a conductivity phase-detection technique, which sets no-slip velocity between the water flow and bubbles and be able to describe the flow characteristics of highly aerated flows (Wang & Chanson 2019; Wang *et al.* 2021; Bai *et al.* 2022).

This study initially establishes five flow scenarios with a slope of $S = 0.01$ to examine the velocity distributions on the gravel-bed. Subsequently, experiments were conducted at a slope of $S = 0.16$, where the ratio of h/D_{84} still exceeds 1, to investigate the variations in velocity and turbulent kinetic energy distributions compared to those observed on planar smooth bed surfaces. The objectives of this study are:

1. To propose a hybrid model for predicting flow velocity profiles in mountainous channels by coupling surface and subsurface flows.
2. To calculate flow resistance based on the new formula and discuss its implication on sediment transport in mountainous river channels.

METHODS

Experimental setups

Experiments were conducted to investigate the hydraulics of flow over a rough bed surface across a range of conditions relevant to mountainous rivers. The experiments were conducted in a tilting flume featuring smooth glass walls, with dimensions of 10 m × 0.3 m × 0.5 m for length, width, and depth, located at the State Key Laboratory of Hydraulics and Mountain River Engineering at Sichuan University (Figure 1(a)). The flume bed was paved with natural cobbles ($D_{50} = 45$ mm and $D_{84} = 63$ mm) (Figure 1(b)). These sediment sizes were selected to ensure high roughness Reynolds numbers ($Re_{k_s} = u_* k_s/\nu$; Table 1), consistent with typical mountain streams. Those cobbles were affixed to the flume floor using a thin epoxy coating, preventing bed load transport and the formation of bedforms (e.g., alternating bars or step pools).

Five experiments were performed using the same bed, with varying channel-bed slopes ($0.006 < S < 0.16$). All flows were fully turbulent ($\mathrm{Re} = Uh/\upsilon > 10^3$). The Froude numbers ($\mathrm{Fr} = U/\sqrt{gh}$) are in a range of 0.34–4.9, i.e., both subcritical and supercritical are considered. Shields numbers ($\tau_* = u_*^2/RgD_{50}$, where $R = 1.65$ is the submerged specific density of sediment) in our experiments are in a range of 0.02–0.1. The experiment scenarios are summarized in Table 1.

Velocity measurement

A downward-looking ADV was employed to measure the vertical velocity distribution along the centerline of the flume's experimental section (Figure 1(c)). Data from the ADV were collected in four experiment sets, representing conditions with gentle slopes. However, at a bed slope of $S = 0.16$, the flow became excessively shallow, fast, and aerated, hindering accurate ADV measurements. Consequently, a dual-tip conductivity phase-detection probe (Bai *et al.* 2022) was utilized for this condition, a tool commonly used in high-energy, shallow, and air mixed streams (Figure 1(d)). The probe, manufactured by The University of Queensland, consisted of two side-by-side needle-shaped sensors of different lengths at the probe's forefront. The phase-detection probe is consistently positioned on the centerline of the flume. Probe displacement in the normal direction is monitored by a mechanical vernier caliper mounted on the probe bracket, with an approximate accuracy of 0.2 mm.

Spatial averaging of velocity profiles was not performed in this study, which will inevitably introduce shape stresses. However, as the ADV-measured velocity profiles were obtained at a uniform position in the flume and the phase-detection probes measured velocity profiles along the flume's centerline (Figure 1(b)), comparisons between these profiles were made to mitigate variations in hydraulic and bed roughness. The ADV was mounted on a vertical screw rod (Figure 1(c)), allowing measurements perpendicular to the flume, with a vertical accuracy of 2 mm. The top of the bed surface ($z = 0$) was defined as a location 45 mm above the flume bottom of the observation section, with the thickness of the subsurface flow (η) set to 45 mm (Figure 3). Since the cobbles are tightly bound to the bottom of the flume, the exchange layer height P was set to

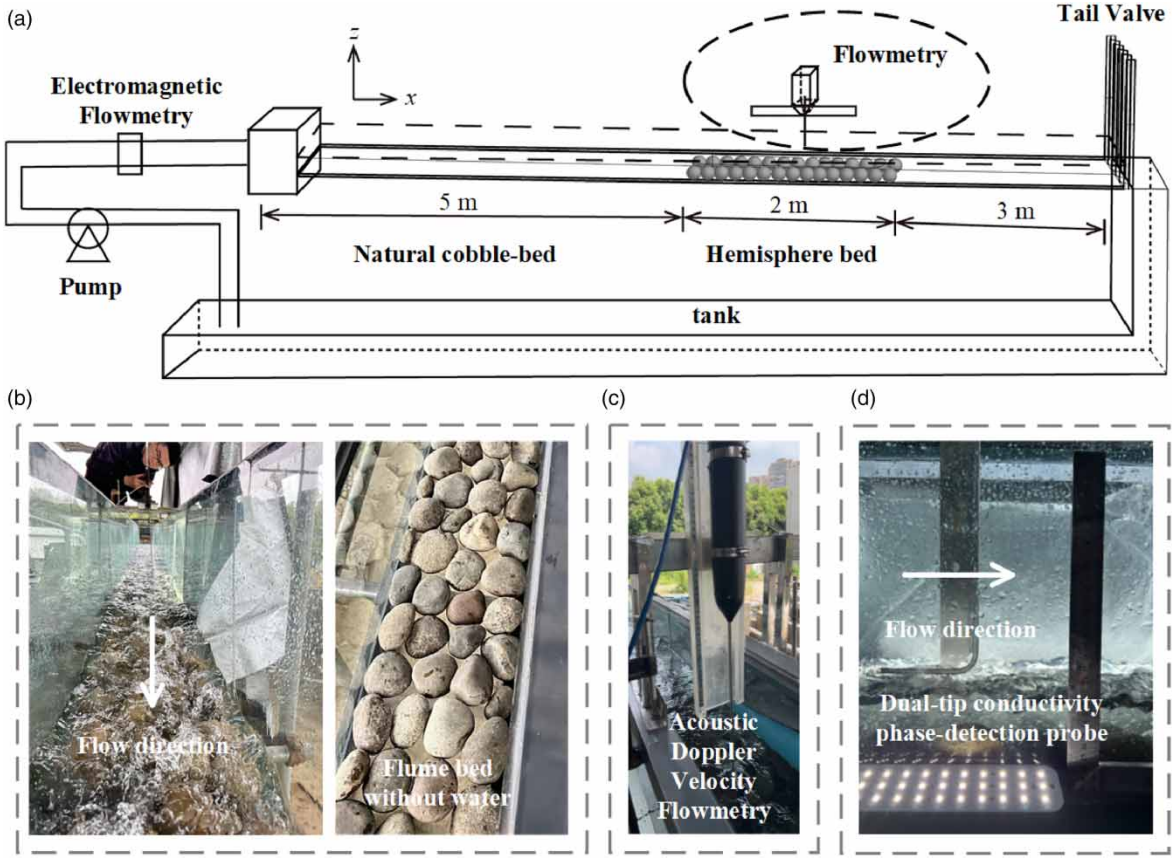

Figure 1 | Overview of experimental setup: (a) Sketch of the flume setting. x denotes the downslope coordinate parallel to the flume bed surface, the z axis is normal to the bed and (b) view looking upstream in the flume bed with shallow flow at $S = 0.16$, $Q = 45$ m^3/h and arrangement of flume bed without water. Instrumentations: (c) acoustic Doppler velocity flowmetry and (d) dual-tip conductivity phase-detection probe.

Table 1 | Summary of experiment scenarios

Exp. #	Bed slope, S	Discharge Q (m^3/h)	Flow Reynolds number, Re ($\times 10^4$)	Roughness Reynolds Number, Re_{k_s} ($\times 10^4$)	Froude number, Fr	Flow depth, h (m)	Shields number, τ_*
1	6‰	196	18.9	2.05	0.37	0.28	0.02
2	8‰	184	17.3	2.36	0.34	0.27	0.03
3	10‰	198	18.9	2.52	0.45	0.25	0.04
4	12‰	195	18.6	2.84	0.37	0.28	0.04
5	160‰	45	4.2	3.15	1.8	0.025	0.05
6	160‰	55	5.1	3.62	4.1	0.035	0.07
7	160‰	65	6.0	4.25	4.9	0.045	0.1

23 mm. Within this layer, the subsurface flow is strongly influenced by shear from surface layer and turbulence (Lamb *et al.* 2017b; Rousseau & Ancey 2020). Flow between $z = 0$ and -P was not measured due to the limitations of the phase-detection probe reaching this area. Rulers were placed along the flume to record differences in height between the water surface and the terrain, used to calculate water depth. The average water depth of the observation section was determined by averaging measurements from the inlet, middle, and outlet sections. Experimental water depths ranged from $0.025 < h < 0.28$ m. An

electromagnetic flowmetry installed in the inlet pipe of the upstream flume measured flow. Average velocity (U) was calculated using the continuity principle, with the formula $U = Q/(W(h+P))$, where $W = 0.3$ m is the flume width and P is the thickness of exchange layer. A honeycomb energy dissipator was placed in the upstream pool to regulate the flow, and a tail valve controlled the outlet opening and the downstream water level, ensuring uniform flow in the observation section.

For each ADV vertical velocity distribution in the experiment, measurement points on each line were determined based on the data quality of the observation point at that time. If a blind spot appeared, measurements were moved to the next point. Velocities in three directions were collected at each measurement point for more than 2 minutes at a sampling frequency of 200 Hz, and 44-μm silicon sand was sprinkled upstream to improve the signal-to-noise ratio. Filtering of collected data was performed based on a correlation coefficient greater than 80 in three directions and a signal-to-noise ratio greater than 20, using the Hampel method to identify outliers before median filtering. When a certain direction was removed, points in all three directions were deleted. Similar to findings by Lamb *et al.* (2017b), the experiment identified an expected slope of −5/3 in the energy spectrum density diagram near the inertial subregion of turbulent flow after filtering, indicating the credibility of the filtering scheme (Figure 2(a)).

For the calculation of air-water flow velocity based on the phase-detection probe signals, the Adaptive Window Cross-Correlation (AWCC) processing method was adopted, in which the phase-detection signal was divided into a series of small, adaptive windows containing a fixed number of bubbles (Kramer *et al.* 2018). The interface velocity in each window was calculated based on the time lag of maximum signal cross-correlation between the two sensor tips. When the width of an adaptive window was sufficiently narrow, the velocity approximated instantaneous velocity, permitting estimate of velocity fluctuations. Although signal segmentation did not guarantee bubble matching between signals from the two sensors, a filtering criterion was set to exclude unrelated segments:

$$\frac{R_{max}}{1 + SPR^2} < A \tag{1}$$

where R_{max} represents the maximum cross-correlation coefficient, and SPR denotes the ratio of the second peak value in the correlation function to R_{max}. A denotes a threshold, below which signal segments with suboptimal correlation (Kramer *et al.* 2018; Bai *et al.* 2022) are discarded. In this study, the number of particles in each window is set to $N_p = 10$, while A is chosen as 0.4. The method of calculating the turbulence interface velocity u_{rms} for the remaining signal segments is as

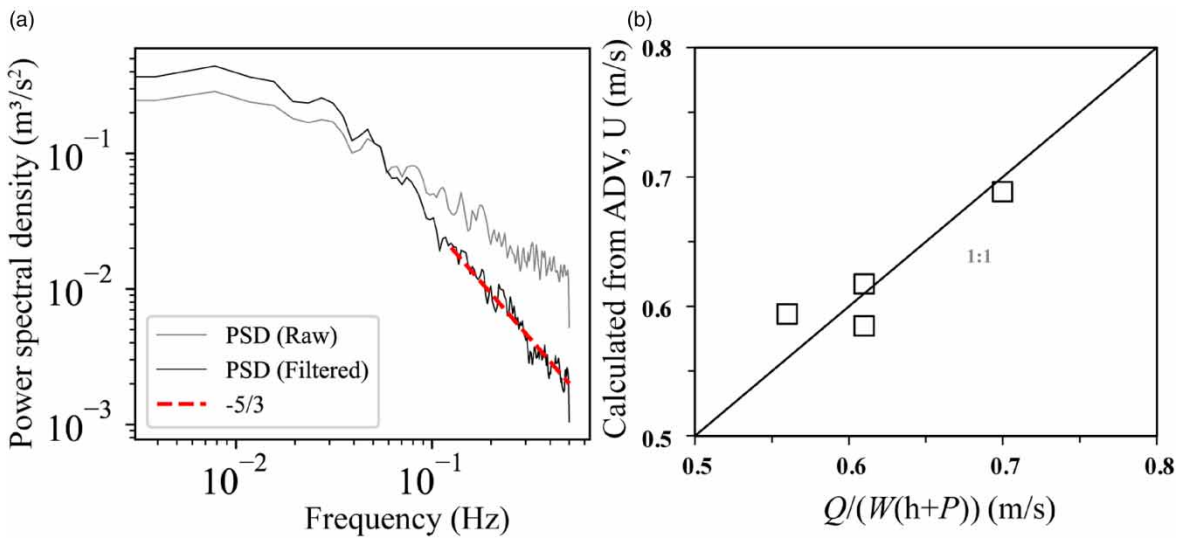

Figure 2 | (a) In the ADV experimental measurements, both the raw spectral density (gray) and the filtered spectral density (black) are shown. The red dashed line represents the −5/3 slope, which appears in the inertial subrange of turbulence. (b) The depth-averaged flow velocity is calculated using electromagnetic flow meters versus ADV.

follows:

$$u_{rms} = \sqrt{\frac{\sum (u_i - \bar{u}) w_i}{\sum w_i}} \tag{2}$$

where u_i represents the velocity of the ith window, and w_i refers to the weight of the window duration, whereas $\bar{u}$ is the average of the remaining velocities u_i weighted by w_i.

In Figure 2(a), the gray curves represent ADV-measured data filtered based on the correlation coefficients and signal-to-noise ratio for the three axes, while the black curves depict data with anomalies removed and median-filtered using the Hampel method. All ADV data in our experiment went through this same process to ensure uniform data quality. Additionally, by comparing the velocity calculated via vertical integration of time-averaged velocities from all measurement points above the bed and the average velocity calculated from the electromagnetic flowmeter in the upstream pool pipeline we see consistency. The distribution of depth-averaged velocities obtained from the ADV verticals and those derived from flow rate calculation equations can be seen in Figure 2(b). The comparison shows that the two methods align well.

THEORETICAL DERIVATION

Improved hybrid mixing length model

The velocity profile formula for surface water flow is initially derived using a mixed length approach, which is improved from Lamb *et al.* (2017b). In this approach, the hydraulic regime of mountainous river channels is divided into two zones: surface layer and subsurface layer, with the average bed elevation serving as the boundary (Figure 3). With the Boussinesq eddy viscosity hypothesis, the Reynolds stress (τ), which quantifies the vertical momentum exchange, is obtained

$$\tau = \rho u_*^2 \left(1 - \frac{z}{h}\right) = \rho \varepsilon d\bar{u}/dz \tag{3}$$

where ε is the eddy viscosity, $\bar{u}$ is the local mean velocity, $u_* = \sqrt{ghS}$ is bed shear velocity, ρ is the fluid density and h is the depth of the surface layer. Following Prandtl's hypothesis, the eddy viscosity can be estimated as the product of local turbulence velocity and length scales.

$$\varepsilon = u_* \left(1 - \frac{z}{h}\right) L_t \tag{4}$$

$$L_t = \kappa z + \alpha_1 k_s \tag{5}$$

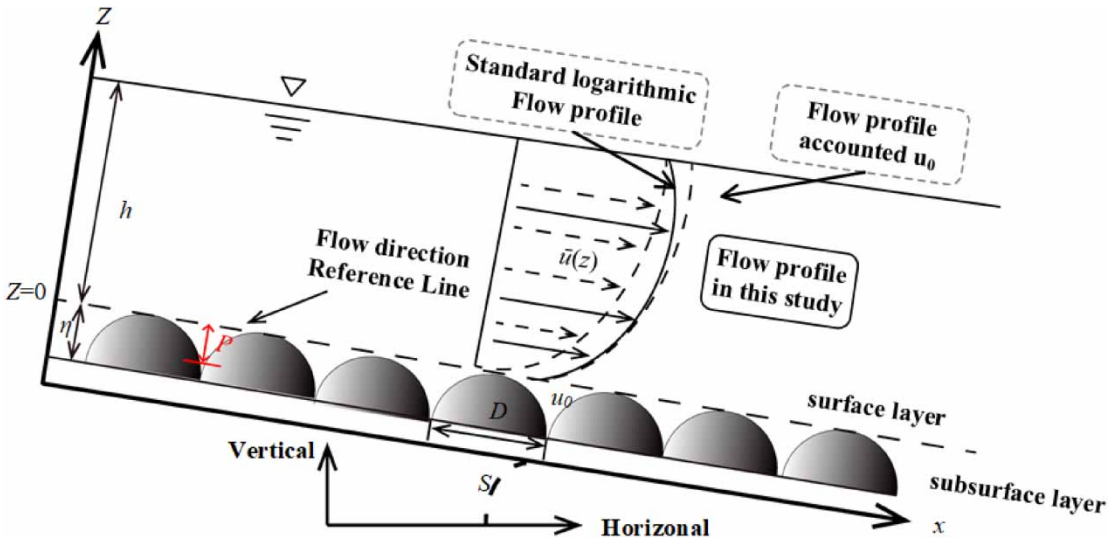

Figure 3 | Conceptual diagram of zones of flow for the surface layer ($z > 0$) and subsurface layer ($z < 0$) over a rough, permeable bed. The bed slope is S, h is the average flow depth, η is the thickness of the subsurface layer, P is the thickness of the exchange layer, D is the diameter of the cobbles, $\bar{u}(z)$ is the downstream flow velocity averaged over turbulence, and u_0 is the $\bar{u}(z)$ at $z = 0$.

where L_t is the mixing length scale, $\kappa = 0.41$ is the von Karman constant coefficient, $\alpha_1 k_s$ means the length dominated by wakes shed from roughness elements and α_1 is a constant less than 1 (Wiberg & Smith 1991; Lamb *et al.* 2017b). For particle roughness, $k_s \approx 2.5D_{84}$ is used in this study (Kamphuis 1974; Lamb *et al.* 2017b). To take into account the impact of the roughness layer on the surface layer, the mixing length l is treated as a sum of two components, given as a hybrid mixing length model. Equations (3), (4), and (5) can be combined and integrated to obtain

$$\frac{\bar{u}(z)}{u_*} = \frac{1}{\kappa}\ln\left(1 + \frac{\kappa z}{\alpha_1 k_s}\right) + \frac{u_0}{u_*} \tag{6}$$

where boundary condition $\bar{u}(z = 0) = u_0$ is applied, with u_0 not being zero at the bed surface of the steep-slope gravel permeable bed.

In Figure 3, the hybrid mixed length formula considers the variation of flow velocity within the subsurface flow and the roughness height. Building upon this, the formula is improved in this study to account for the influence of roughness elements on the velocity distribution near the water surface. The empirical divergence function is used to describe the dip and S-shaped distribution of vertical water flow structure under large roughness (Ferro & Baiamonte 1994; Ferro & Pecoraro 2000). In this study, the form of the function has been modified based on previous research, considering only the flow structure above the height ($z = 0.1k_s$) corrected by Equation (7), in which b_1 is the number estimated by using velocity measurements.

$$\frac{\bar{u}(z)}{u_*} = \frac{1}{\kappa}\ln\left(1 + \frac{\kappa z}{\alpha_1 k_s}\right) + \frac{u_0}{u_*} + b_1\left(\log\frac{k_s}{z} - 1\right)^9 \tag{7}$$

where $b_1(\log k_s/z - 1)^9$ is the empirical divergence function.

The depth-averaged flow velocity ($U = 1/h\int_0^h \bar{u}(z)\mathrm{d}z$) of surface layer can be obtained by integrating from $z = 0$ to h and then dividing by h. For the vertical profile the mean value U/u_* has the following expression:

$$\frac{U}{u_*} = \frac{1}{\kappa}\left[\left(1 + \frac{\alpha_1 k_s}{\kappa h}\right)\ln\left(1 + \frac{\kappa h}{\alpha_1 k_s}\right) - 1\right] + \frac{u_0}{u_*} + \frac{b_1}{h}\mathrm{X}_9\left(\frac{z}{k_s}\right)\Bigg|_0^h \tag{8}$$

$$\mathrm{X}_9\left(\frac{z}{k_s}\right) = \frac{z}{k_s}\sum_{j=0}^{9}\frac{9!}{j!(\ln 10)^{9-j}}\left(\log\frac{k_s}{z} - 1\right)^j \tag{9}$$

in which $|_0^h$ indicates that the function has to be calculated for the integration range and $\mathrm{X}_9(z/k_s)$ has to be calculated by Equation (9).

Model performance evaluation

The Nash–Sutcliffe Efficiency (NSE) coefficient and Root Mean Square Error (RMSE) are commonly used to evaluate hydrological and hydraulic models, and their formulas are as follows:

$$\mathrm{NSE} = 1 - \frac{\sum_{i=1}^{i=n}(\widehat{Y}_i - Y_i)^2}{\sum_{i=1}^{i=n}(Y_i - \bar{Y})^2} \tag{10}$$

$$\mathrm{RMSE} = \sqrt{\frac{\sum_{i=1}^{i=n}(\widehat{Y}_i - Y_i)^2}{n}} \tag{11}$$

where $\widehat{Y}_i$ and Y_i represent the predicted and measured data of the dependent variable Y, respectively; $\bar{Y}$ denotes the mean measured values of Y; n is the sample size. It is important to note that the NSE indicates how closely the plot of predicted data aligns with the observed data on the 1:1 line. When NSE = 1, it indicates that the model explains all the variation in the measurements, whereas NSE = 0 suggests that the model predictions are as accurate as the mean of the observed values. A negative NSE indicates unreliable predicted results. The RMSE quantifies the degree of dispersion between model predictions and observed values.

RESULTS

Surface flow velocity profiles

Figure 4 illustrates the distribution of surface layer velocity profiles, with the red line representing the resulting curve fit via Equation (7). Specifically, Figure 4(a)–4(d) demonstrate the flow velocity distribution under slope conditions of 0.006–0.012, while Figure 4(e)–4(g) displays the flow velocity distribution under a slope condition of 0.16 with respective flow rates of 45, 55 and 65 m^3/h.

When the slope is gentle, the coefficient b_1 of the divergence function in all the flow velocity profiles in Figure 4(a)–4(d) is not zero. Conversely, b_1 equals zero for the downstream flow velocity profiles under conditions where the slope is 0.16. Table 2 records the values of α_1, b_1 for all fitted curves in Figure 4.

In general, the velocity predicted by the equation that considers near-bed flow closely corresponds with the measured velocity, particularly apparent for experiments where the near-bed flow incurs when the bed slope is larger. Evident in Fi(g)ures 4(a)-(g) under the experimental conditions of changing slope and relative roughness, all velocity profiles essentially comply with the predictions granted by the equation, factoring in the near-bed flow and the near-surface flow dip. The larger the decrease in near-surface velocity, the larger the value of b_1.

The mixed length sheds light on the departure of the logarithmic linear region velocity profile near the bed from the logarithmic velocity profile. The incorporation of near-bed flow velocity accounts for the deviation induced by higher subsurface flow velocity, whereas the divergence function elucidates the departure of reduced flow velocity higher from the roughness

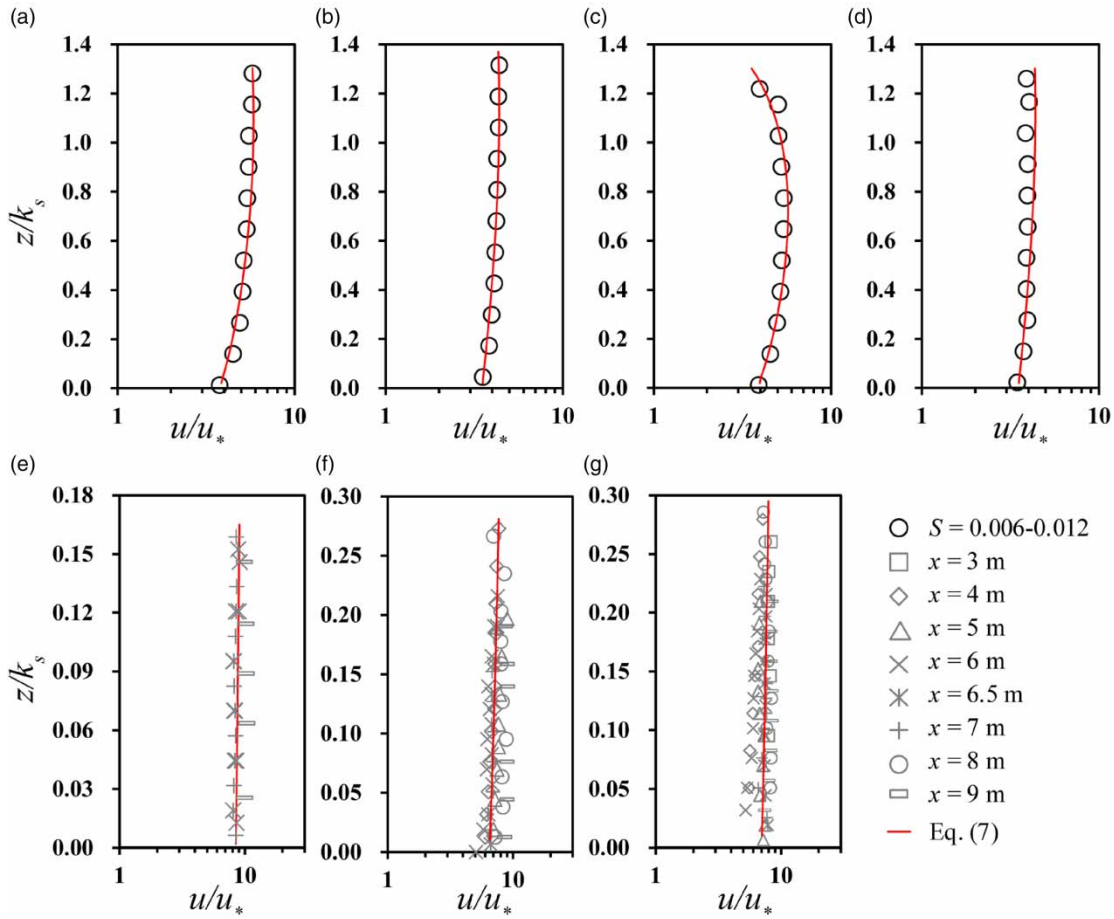

Figure 4 | Dimensionless velocity profiles for seven experiments with ADV and phase-detection probes: (a) $S = 0.006$, (b) $S = 0.008$, (c) $S = 0.01$, (d) $S = 0.012$, (e) $S = 0.16$ and $Q = 45$ m^3/h, (f) $S = 0.16$ and $Q = 55$ m^3/h, (g) $S = 0.16$ and $Q = 65$ m^3/h. The red line is the improved hybrid mixing length model for different α_1 and β_1.

Table 2 | The fitting parameters α_1, β_1 and fitting goodness in Figure 4

Exp #	Bed slope, S	α_1	β_1	k_s/h	NSE
1	6‰	0.25	0.3	0.56	0.82
2	8‰	0.8	0.15	0.58	0.90
3	10‰	0.23	1.0	0.63	0.71
4	12‰	0.7	0.4	0.56	0.34[a]
5	160‰	0.25	0	6.3	0.02
6	160‰	0.18	0	4.5	0.11
7	160‰	0.25	0	3.5	0.03

[a]α_1 is larger than 1.

height k_s. In Figure 4(d), at 0.4 to 0.8k_s the predicted velocity is higher than the measured velocity. When α_1 is greater than 1, we can fit the vertical distribution well, but its influencing factors cannot be explained.

Turbulence intensities

Figure 5(a)–5(d) illustrates the fluctuations in flow velocities in three directions and the normalized Reynolds stress ($-\overline{u'\omega'}/u_*^2$) in the downstream direction for slopes in the range of 0.006–0.012. Figure 5(e)–5(g) depicts changes in

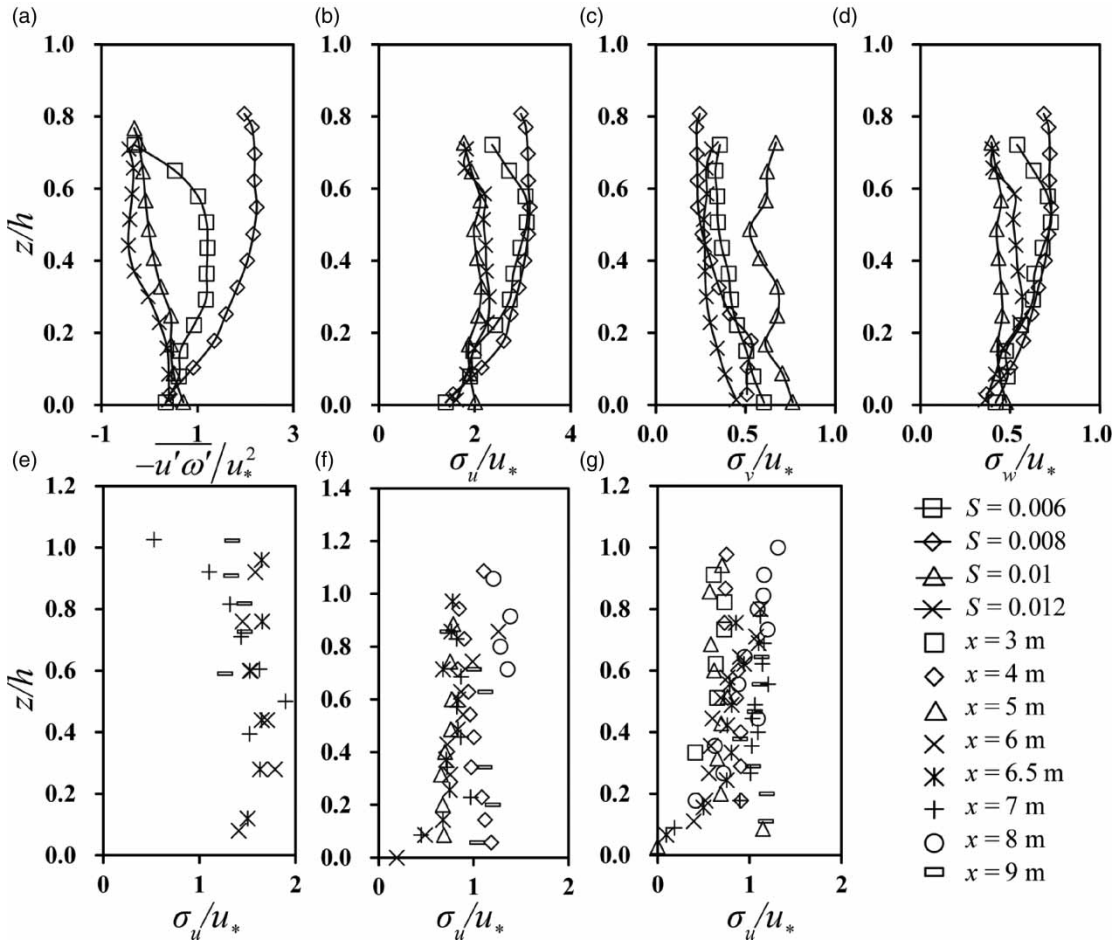

Figure 5 | Profiles of (a) normalized Reynolds stresses, and turbulence intensities in the (b) downstream ($\sigma_u = \sqrt{(u'^2)}$), (c) transverse ($\sigma_v = \sqrt{(v'^2)}$), bed-normal ($\sigma_\omega = \sqrt{(\omega'^2)}$), and (e, f, g) downstream ($S = 0.16$ for different discharges, in which $\sigma_u = u_{rms}$) directions as a function of normalized height above the bed. Data are for all seven experiments.

dimensionless turbulence intensity in the downstream direction for the air-water interface velocity derived from the AWCC method when the slope is 0.16 and the flow rates are 45, 55, and 65 m^3/h, respectively. In Figure 5(a), there are no significant extrema for the Reynolds stress. Similar to the pattern observed on a smooth bed, the Reynolds stress decreases with increasing water depth at a slope of 0.006. However, it increases and stabilizes at a slope of 0.008 before decreasing near the water surface. Yet, under conditions where the slope is 0.01 and 0.012, values less than zero surface at 0.3 and 0.5 h – situations that emerge after the maximum flow velocity in the velocity profile starts to decrease. At times like these, when $h/D_{84} = 2$–3, it is evident that the influence of the bed particle size on water flow is significant. Franca (2005) suggests that this change in distribution is due to the wake effect of bed form morphology.

The change in downstream turbulence intensity, as depicted in Figure 5(b), 5(e) and 5(f), reveals a trend of increased intensity from near-bed to 0.2 h, regardless of the considerable variation in slope and flow rate. This may be attributed to the rough particles near the bed impeding water turbulence. For a water depth exceeding 0.2 h, a slight decrease adjacent to the water surface is noticed only in conditions with $S = 0.006$–0.012, whereas with $S = 0.16$, no significant decrease is observed near $z/h = 1$ in Figure 5(e)–5(g), indicating the influence of rough bed elements extends across the entire water depth. The cross-flow turbulence intensity of the flume decreases with increasing water depth, with a maximum value near the bed of approximately 0.6, showing no strong correlation with channel slope. The vertical turbulence intensity in the flume is generally lower than the turbulence intensity of 1 under smooth bed conditions. This suggests that bed rough elements and surface wave action may have a significant impact on the vertical turbulence intensity.

Depth-averaged flow and friction factor

In river engineering, the flow resistance of water flow significantly influences the average flow velocity and sediment transport. The ratio of depth-averaged flow velocity to bed shear rate can be used to describe flow resistance. To assess the performance of our formula in actual mountainous river flows, we compared it with the Ferguson (2007) formula,

$$\frac{U}{u_*} = \frac{7.5 \times 2.36 h/D_{84}}{\sqrt{7.5^2 + 2.36^2 (h/D_{84})^{5/3}}} \tag{12}$$

Figure 6 illustrates the relationship between the flow resistance calculated using our formula, those obtained from measurements, and the Ferguson formula. The fitting goodness of the results is quantitatively indicated by NSE and RMSE (information in Table 3). Overall, the flow resistance derived from our formula and Ferguson's formula closely matches the measured values. Analysis based on the NSE Coefficient and RMSE indicates that both Equations (8) and (12) tend to overestimate the flow resistance overall, particularly under high relative roughness conditions. However, when considering the influence of roughness on vertical flow velocity, both our formula and Ferguson's formula exhibit a good fit with the measured coefficients. Since the Ferguson's formula is based on field measurements, the similarity between our experimental formula and that of Ferguson's suggests that laboratory-derived flow resistance formulas can effectively reflect flow resistance in field river channels.

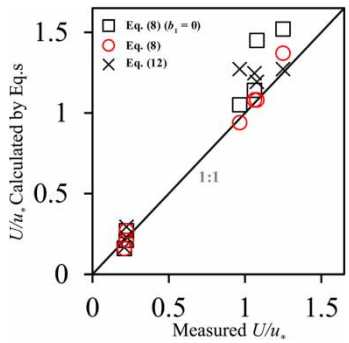

Figure 6 | The U/u_* relationships between different flow resistance equations and measured data. Comparison between the formula proposed by Lamb *et al.* (Equation (8) with $b_1 = 0$), Ferguson (Equation (12)), and the formula presented in this study (Equation (8)). The squares are the values of Equation (8) under the assumption of negligible surface wave or secondary flow. The red circles represent the values of Equation (8) and the crosses represent the values of Ferguson which matched well observations in steep mountain river channels.

Table 3 | Nash–Sutcliffe Efficiency Coefficient and root mean square error in Figure 6

Index	Equation (8) ($b_1 = 0$)	Equation (12)	This study
NSE	0.80	0.89	0.97
RMSE	0.19	0.15	0.08

DISCUSSION

Flow velocity profiles

This study proposes a velocity profile equation that considers the interaction between the roughness layer, near-bed flow velocity, and the dip near the surface. This solution better aligns with our observations compared to previous models presented by Lamb *et al.* (2017b) and Luo *et al.* (2022). The mixed length model allows deviations from the logarithmic profile within the roughness layer and effectively models the reduction in flow velocity experienced in channels, slopes, and other subsurface flow. While many studies suggest that the decrease in velocity near the flow surface is due to surface wave (Emmett 1970), our experiments show that when the slope $S = 0.16$, the effect of surface wave was more pronounced than in cases where $S = 0.006$–0.012, yet the velocity near the flow surface did not decrease significantly.

This discrepancy may be attributed to the contrast in pore and permeability between hillslope and mountain river flow, with the transition from surface water flow to subsurface being smoother in our experimental setup. In our steep-slope experiments, the subsurface velocity was much larger than in the hillslope flow experiments, preventing a reduction in near-surface velocity under shallow flow conditions on steep slopes. As the slope changes, our experiment visually depicts a transition from a relatively steady and uniform water surface to aerated supercritical flow on steep slopes. Despite variations in bed slope or flow conditions, the vertical velocity distribution above the bed can be predicted using a mixed length model ($b_1 = 0$) below the maximum velocity from verticals, considering the mixed length and near-bed flow velocity. While this result suggests that the velocity within the roughness layer is insensitive to relative roughness but responds sensitively to changes in subsurface flow velocity, it supports the findings of Lamb *et al.* (2017b), but contradicts the assumption presented by Recking (2009).

Although our model, incorporating a divergence function, fits well with the velocity dip near the flow surface, a decrease in velocity was not observed under the steep-slope conditions in our experiment. This implies that the divergence function may not significantly correlate with surface wave.

Implications for sediment transport

The flow resistance of mountainous river channels is influenced by factors such as form drag, grain roughness, and bed structure. There may be significant differences in the sediment transport relationship derived from relative roughness between mountainous river channels and hillslope flow. While most studies focus on the relationship between relative roughness and flow resistance, the presence of bed surface structures in plain rivers may also lead to a reduction in the sediment transport relationship, with little change in relative roughness (Zhang *et al.* 2021).

Bed surface structures can have a significant impact on sediment transport, especially in cases involving the formation of aggregates or large boulders (Li *et al.* 2023a). However, there is insufficient evidence to support the claim that bed surface structures are the primary cause of increased flow resistance in mountainous river channels (Lamb *et al.* 2017b). Emmett (1970) conducted experiments in rivers with gradients exceeding 17‰ and found that the water flow turbulence was significant. Ferro & Pecoraro (2000) found that the flow resistance, derived using the incomplete self-similarity method, is not only related to the relative roughness, but also to the Re.

Additionally, based on our experimental results and referring to Lamb *et al.* (2008), the formula derived shows that near-bed turbulence intensity varies linearly with mean flow velocity (Figure 5(b)). In our study, the decrease in measured flow resistance is mainly due to the reduction in turbulence intensity compared to that in fluvial rivers, leading to a decrease in mean flow velocity and an increase in the flow resistance, stabilizing sediment transport on the slope.

When the flow is subcritical, the relative roughness in our experiment remains relatively constant, and the flow resistance also remains stable. This indicates that in subcritical flow, the flow resistance is mainly related to the relevant roughness, which is consistent with the conclusion of Flammer *et al.* (1970). However, this calculation does not consider the effects

of surface fluctuations, resulting in a slightly higher calculated flow resistance than the measured value. This is different from the conclusion that surface wave fluctuations enhance flow resistance (Emmett 1970). Here, Combining Equations (3)–(5), where $L_t = \kappa z$, we can obtain the formula commonly used in low gradient rivers,

$$\frac{\bar{u}(z)}{u_*} = \frac{1}{\kappa}\ln\left(\frac{z}{k_s}\right) + B \tag{13}$$

where B is the integration constant.

Due to the roughness layer in surface water flow not conforming to the logarithmic velocity distribution, Figure 7 plots the vertical velocity distribution from approximately 0.1 h (0.18k_s). Figure 7 shows the dimensionless relationship between flow velocity and dimensionless height. The triangles in the figure represent the experimental data for the Exp. 3. The two dot-dashed lines (1 and 2) represent the logarithmic velocity profile formula (Equation (13), with B equal to 4.5 and 8.5 for 1 and 2, respectively), and Equation (7) ($b_1 = 0$) is depicted as the dashed line 4. The solid line 3 represents the formula introduced in this study after incorporating the divergence function (Equation (7)). The gray area between the dashed 4 and dot-dashed line 2 represents the flow resistance due to roughness height (k_s) (Lamb *et al.* 2017b), while the grid area between the solid 3 and dashed line 4 represents the flow resistance due to surface wave fluctuations or secondary flow (Finley *et al.* 1966; Ferro & Baiamonte 1994; Ferro 2003). Additionally, the slope in this experiment is not sufficient to generate roll waves (Emmett 1970). The arrows between the dot-dashed line 1 and the solid line 3 represent the increase in velocity relative to the logarithmic profile ($B = 4.5$). Although Equation (7) ($b_1 = 0$) can better represent the case where near-bed flow velocity is not zero due to subsurface flow, it overestimates the velocity in the vicinity of the water surface, as indicated by the grid area in the Figure 7. This is also why the U/u_* calculated by the mixed length model (Equation (8) ($b_1 = 0$)) is higher than the measured flow resistance when the relative roughness is high (Figure 6). In Figure 4, the value of b_1 for Figure 4(c) is larger than that for Figure 4(d). This is because Figure 4(c) has a higher flow rate and shallower water depth, resulting in a greater influence of secondary flow.

CONCLUSIONS

The flow velocity profiles on an experimental gravel-bed under different slopes were measured using ADV and a phase-detection probe. Analysis was conducted within a slope range of 0.006–0.16, and flow discharges ranging from 0.01 to 0.06 m^3/s. The variations in turbulent intensity and flow resistance parameters were examined. The following conclusions were drawn:

1. The newly developed formulae for flow velocity profiles, considering factors such as near-bed velocity, mixed length under roughness scale, and velocity dip near the water surface, matches well with the measured data.

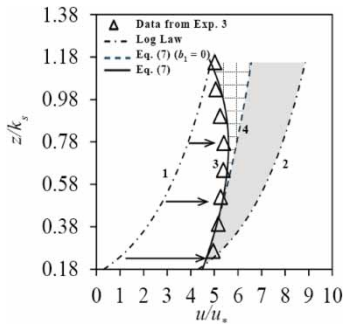

Figure 7 | The dimensionless relationship between flow velocity and dimensionless height. The triangles in Figure 7 represent the experimental data for Exp. 3. The two dot-dashed lines represent the logarithmic velocity profile formula (Equation (13), in which the B is 4.5 and 8.5 for 1 and 2, respectively) and Equation (7) ($b_1 = 0$) is the dashed line 4; the solid line 3 represents the formula introduced in this study after incorporating the divergence function (Equation (7)). The gray area between the dashed 4 and dot-dashed line 2 represents the flow resistance due to roughness height (k_s), while the grid area between the solid 3 and dashed line 4 represents the flow resistance due to surface wave fluctuations or secondary flow. The arrows between the dot-dashed 1 and solid line 3 represent the increase in velocity relative to the logarithmic profile ($B = 4.5$).

2. Relative large-scale roughness leads to deviations in the peak positions of turbulent intensity and Reynolds stress from those of a smooth bed surface. Turbulent intensity downstream tends to distribute uniformly across the entire water depth.
3. The flow resistance formula obtained through integration, similar to the ones derived from field measurements in mountainous river channels, aligns well with the measured flow resistance. This suggests that laboratory-scale water flow resistance experiments effectively reflect macro-scale resistance variations. Furthermore, the mixed length formula may overestimate the flow resistance in mountainous river channels due to surface wave fluctuations or secondary flow.

In conclusion, this study highlights the significance of subsurface flow in the velocity profile of mountainous river channels. The limitations of the present study primarily arise from two aspects. Firstly, we did not consider the influences of bed cobble arrangements in our experiment, which brings bed micro-structures and variations in porosity, thereby affecting the parameter α_1 in Equation (7) according to Luo *et al.* (2022). Secondly, our experiment lacks measurements of subsurface flow velocities, preventing the establishment of a direct relationship between velocity profiles and subsurface pore flow. These aspects need to be considered in future research.

ACKNOWLEDGEMENTS

This study was supported by the National Key Research and Development Program of China (2022YFC3203903) and the National Natural Science Foundation of China (No. 52279077). The authors would like to thank Dr Xiaojuan Deng for her help on the figures.

DATA AVAILABILITY STATEMENT

Data cannot be made publicly available; readers should contact the corresponding author for details.

CONFLICT OF INTEREST

The authors declare there is no conflict.

REFERENCES

Abrahams, A. D. & Parsons, A. J. 1994 Hydraulics of interrill overland flow on stone-covered desert surfaces. *Catena (Giessen)* **23** (1), 111–140. https://doi.org/10.1016/0341-8162(94)90057-4.

Bai, R., Bai, Z., Wang, H. & Liu, S. 2022 Air-water mixing in vegetated supercritical flow: Effects of vegetation roughness and water temperature on flow self-aeration. *Water Resources Research* **58** (2), e2021WR031692. https://doi.org/10.1029/2021WR031692.

Barry, J. J., Buffington, J. M. & King, J. G. 2004 A general power equation for predicting bed load transport rates in gravel bed rivers. *Water Resources Research* **40** (10). https://doi.org/10.1029/2004WR003190.

Bathurst, J. C. 1988 *Velocity Profile in High-Gradient, Boulder-bed Channels*.

Bathurst, J. C. 2002 At-a-site variation and minimum flow resistance for mountain rivers. *Journal of Hydrology* **269** (1), 11–26. https://doi.org/10.1016/S0022-1694(02)00191-9.

Behera, P. K., Patel, M., Deshpande, V. & Kumar, B. 2024 Patterns of turbulent flow structures over dune shaped bed features under the influence of downward seepage. *Experimental Thermal and Fluid Science* **153**, 111128. https://doi.org/10.1016/j.expthermflusci.2023.111128.

Byrd, T. C., Furbish, D. J. & Warburton, J. 2000 Estimating depth-averaged velocities in rough -channels. *Earth Surface Processes and Landforms* **25** (2), 167–173. https://doi.org/10.1002/(SICI)1096-9837(200002)25:2<167::AID-ESP66 > 3.0.CO;2-G.

Emmett, W. W. 1970 *The Hydraulics of Overland Flow on Hillslopes: Dynamic and Descriptive Studies of Hillslopes*. US Government Printing Office, Washington, DC.

Ferguson, R. 2007 Flow resistance equations for gravel- and boulder-bed streams. *Water Resources Research* **43** (5). https://doi.org/10.1029/2006WR005422.

Ferro, V. 2003 ADV measurements of velocity distributions in a gravel-bed flume. *Earth Surface Processes and Landforms* **28** (7), 707–722. https://doi.org/10.1002/esp.467.

Ferro, V. & Baiamonte, G. 1994 Flow velocity profiles in gravel-bed rivers. *Journal of Hydraulic Engineering* **120** (1), 60–80. https://doi.org/10.1061/(ASCE)0733-9429(1994)120:1(60).

Ferro, V. & Pecoraro, R. 2000 Incomplete self-similarity and flow velocity in gravel bed channels. *Water Resources Research* **36** (9), 2761–2769. https://doi.org/10.1029/2000WR900164.

Finley, P. J., Phoe, K. C. & Poh, J. 1966 Velocity measurments in a thin turbulent water layer, *La Houille Blanche*, (6), pp. 713–721. Available at: https://doi.org/10.1051/lhb/1966045.

Flammer, G. H., Tullis, J. P. & Mason, E. S. 1970 Free surface, velocity gradient flow past hemisphere. *Journal of the Hydraulics Division* **96** (7), 1485–1502. https://doi.org/10.1061/JYCEAJ.0002563.

Franca, M. J. 2005 Flow dynamics over a gravel riverbed. In *XXXI IAHR Congress*, Seoul, Korea, pp. 6542–6551.

Gupta, A. D. & Paudyal, G. N. 1985 Characteristics of free surface flow over gravel bed. *Journal of Irrigation and Drainage Engineering* **111** (4), 299–318. https://doi.org/10.1061/(ASCE)0733-9437(1985)111:4(299).

Heimann, F. U. M., Rickenmann, D., Turowski, J. M. & Kirchner, J. W. 2015 Sedflow – a tool for simulating fractional bedload transport and longitudinal profile evolution in mountain streams. *Earth Surface Dynamics* **3** (1), 15–34. https://doi.org/10.5194/esurf-3-15-2015.

Hu, Y., Huai, W. & Han, J. 2013 Analytical solution for vertical profile of streamwise velocity in open-channel flow with submerged vegetation. *Environmental Fluid Mechanics* **13** (4), 389–402. https://doi.org/10.1007/s10652-013-9267-6.

Jiang, W., Zeng, L., Fu, X. & Wu, Z. 2022 Analytical solutions for reactive shear dispersion with boundary adsorption and desorption. *Journal of Fluid Mechanics* **947**, A37.

Kamphuis, J. W. 1974 Determination of sand roughness for fixed beds. *Journal of Hydraulic Research* **12** (2), 193–203. https://doi.org/10.1080/00221687409499737.

Kramer, M., Valero, D., Chanson, H. & Bung, D. B. 2018 Towards reliable turbulence estimations with phase-detection probes: An adaptive window cross-correlation technique. *Experiments in Fluids* **60** (1), 2. https://doi.org/10.1007/s00348-018-2650-9.

Lamb, M. P., Dietrich, W. E. & Venditti, J. G. 2008 Is the critical Shields stress for incipient sediment motion dependent on channel-bed slope? *Journal of Geophysical Research: Earth Surface* **113** (F2). https://doi.org/10.1029/2007JF000831.

Lamb, M. P., Brun, F. & Fuller, B. M. 2017a Direct measurements of lift and drag on shallowly submerged cobbles in steep streams: Implications for flow resistance and sediment transport. *Water Resources Research* **53** (9), 7607–7629. https://doi.org/10.1002/2017WR020883.

Lamb, M. P., Brun, F. & Fuller, B. M. 2017b Hydrodynamics of steep streams with planar coarse-grained beds: Turbulence, flow resistance, and implications for sediment transport. *Water Resources Research* **53** (3), 2240–2263. https://doi.org/10.1002/2016WR019579.

Li, W., Saletti, M., Hassan, M. A., Johnson, J. P., Carr, J., Chui, C. & Yang, K. 2023a The influence of coarse particle abundance and spatial distribution on sediment transport and cluster evolution in steep channels under sediment-starved conditions. *CATENA* **229**, 107199. https://doi.org/10.1016/j.catena.2023.107199.

Li, G., Gong, Z., Jiang, W., Zhan, J., Wang, B., Fu, X., Xu, M. & Wu, Z. 2023b Environmental transport of gyrotactic microorganisms in an open-channel flow. *Water Resources Research* **59** (4), e2022WR033229. https://doi.org/10.1029/2022WR033229.

Lu, Y., Cheng, N.-S. & Wei, M. 2021 Formulation of bed shear stress for computing bed-load transport rate in vegetated flows. *Physics of Fluids* **33** (11), 115105. https://doi.org/10.1063/5.0067851.

Luo, M., Wang, X., Yan, X. & Huang, E. 2020 Applying the mixing layer analogy for flow resistance evaluation in gravel-bed streams. *Journal of Hydrology* **589**, 125119. https://doi.org/10.1016/j.jhydrol.2020.125119.

Luo, M., Ye, C., Wang, X., Huang, E. & Yan, X. 2022 Analytical model of flow velocity in gravel-bed streams under the effect of gravel array with different densities. *Journal of Hydrology* **608**, 127581. https://doi.org/10.1016/j.jhydrol.2022.127581.

Nakagawa, H., Tsujimoto, T. & Shimizu, Y. 1988 Velocity profile of flow over rough permeable bed. In *6th IAHR Congress*, Kyoto, Japan, pp. 449–456.

Nepf, H. & Ghisalberti, M. 2008 Flow and transport in channels with submerged vegetation. *Acta Geophysica* **56** (3), 753–777. https://doi.org/10.2478/s11600-008-0017-y.

Nezu, I. & Rodi, W. 1986 Open-channel flow measurements with a laser Doppler anemometer. *Journal of Hydraulic Engineering* **112** (5), 335–355. https://doi.org/10.1061/(ASCE)0733-9429(1986)112:5(335).

Nikora, V., McEwan, I., McLean, S., Coleman, S., Pokrajac, D. & Walters, R. 2007 Double-averaging concept for rough-bed open-channel and overland flows: Theoretical background. *Journal of Hydraulic Engineering* **133** (8), 873–883. https://doi.org/10.1061/(ASCE)0733-9429(2007)133:8(873).

Qu, L., Lei, T., Zhou, C. & Yang, X. 2023 Measuring sediment transport capacity of concentrated flow with erosion feeding method. *Land* **12** (2), 411. https://doi.org/10.3390/land12020411.

Recking, A. 2009 Theoretical development on the effects of changing flow hydraulics on incipient bed load motion. *Water Resources Research* **45** (4). https://doi.org/10.1029/2008WR006826.

Rickenmann, D. & Recking, A. 2011 Evaluation of flow resistance in gravel-bed rivers through a large field data set. *Water Resources Research* **47** (7). https://doi.org/10.1029/2010WR009793.

Rousseau, G. & Ancey, C. 2020 Scanning PIV of turbulent flows over and through rough porous beds using refractive index matching. *Experiments in Fluids* **61** (8), 172. https://doi.org/10.1007/s00348-020-02990-y.

Roy, A. G., Buffin-Belanger, T., Lamarre, H. & Kirkbride, A. D. 2004 Size, shape and dynamics of large-scale turbulent flow structures in a gravel-bed river. *Journal of Fluid Mechanics* **500**, 1–27. https://doi.org/10.1017/S0022112003006396.

Schneider, J. M., Rickenmann, D., Turowski, J. M. & Kirchner, J. W. 2015 Self-adjustment of stream bed roughness and flow velocity in a steep mountain channel. *Water Resources Research* **51** (10), 7838–7859. https://doi.org/10.1002/2015WR016934.

Tu, H., Tsujimoto, T. & Graf, W. H. 1988 Velocity distribution in a gravel-bed flume. In *Proc., 6th Congress of Asian and Pacific Division of Int. Association of Hydraulic Research*. IAHR, pp. 425–431.

Vedula, S. & Achanta, R. R. 1985 Bed shear from velocity profiles: A new approach. *Journal of Hydraulic Engineering* **111** (1), 131–143. https://doi.org/10.1061/(ASCE)0733-9429(1985)111:1(131).

Wang, H. & Chanson, H. 2019 Characterisation of transverse turbulent motion in quasi-two-dimensional aerated flow: Application of four-point air-water flow measurements in hydraulic jump. *Experimental Thermal and Fluid Science* **100**, 222–232. https://doi.org/10.1016/j.expthermflusci.2018.09.004.

Wang, X. K., Ye, C., Wang, B. J. & Yan, X. F. 2015 Experimental study on velocity profiles with different roughness elements in a flume. *Acta Geophysica* **63** (6), 1685–1705. https://doi.org/10.1515/acgeo-2015-0063.

Wang, H., Liu, X., Bai, R. & Liu, S. 2021 Bubble characteristics affecting air-water exchange in open-channel flow with a jet forming over a sudden bottom drop. *Experimental Thermal and Fluid Science* **124**, 110366. https://doi.org/10.1016/j.expthermflusci.2021.110366.

Wang, Q., Zhang, Y., Wang, P., Feng, T. & Bai, Y. 2023 Longitudinal velocity profile of flows in open channel with double-layered rigid vegetation. *Frontiers in Environmental Science* **10**. Available from: https://www.frontiersin.org/articles/10.3389/fenvs.2022.1094572.

Wiberg, P. L. & Smith, J. D. 1991 Velocity distribution and bed roughness in high-gradient streams. *Water Resources Research* **27** (5), 825–838. https://doi.org/10.1029/90WR02770.

Wu, Z., Jiang, W., Zeng, L. & Fu, X. 2023 Theoretical analysis for bedload particle deposition and hop statistics. *Journal of Fluid Mechanics* **954**, A11.

Yager, E. M., Kirchner, J. W. & Dietrich, W. E. 2007 Calculating bed load transport in steep boulder bed channels. *Water Resources Research* **43** (7). https://doi.org/10.1029/2006WR005432.

Yager, E. M., Dietrich, W. E., Kirchner, J. W. & McArdell, B. W. 2012 Prediction of sediment transport in step-pool channels. *Water Resources Research* **48** (1). https://doi.org/10.1029/2011WR010829.

Zagni, A. F. E. & Smith, K. V. H. 1976 Channel flow over permeable beds of graded spheres. *Journal of the Hydraulics Division* **102** (2), 207–222. https://doi.org/10.1061/JYCEAJ.0004482.

Zhang, S., Zhu, Z., Peng, J., He, L. & Chen, D. 2021 Laboratory study on the evolution of gravel-bed surfaces in bed armoring processes. *Journal of Hydrology* **597**, 125751. https://doi.org/10.1016/j.jhydrol.2020.125751.

First received 4 May 2024; accepted in revised form 15 May 2024. Available online 6 June 2024